J Solid State Electrochem (2012) 16:3275–3288
DOI 10.1007/s10008-012-1762-z

ORIGINAL PAPER

Impedance simulation of a solid oxide fuel cell anode in time domain

R. Mohammadi · M. Ghassemi · Y. Mollayi Barzi · M. H. Hamedi

Received: 4 December 2011 / Revised: 26 April 2012 / Accepted: 28 April 2012 / Published online: 19 May 2012

Abstract The purpose of the current study is to simulate the behavior of a solid oxide fuel cell (SOFC) anode under sinusoidal excitation. The obtained harmonic response is used as a base for electrochemical impedance spectra simulation. The electrochemical impedance spectroscopy (EIS) is a powerful non-destructive tool for SOFC researches. In order to evaluate the EIS experimental results, efforts are devoted to develop EIS numerical simulation tools. In this study, a planar SOFC is modeled, and the steady state behavior and frequency response, as well as the electrochemical spectra of the anode, are obtained. The developed model couples the electrochemical kinetics with mass transport. The Butler–Volmer equation is used for the anode electrochemistry, and the species equations are used for gas transport in the anode channel. In order to solve the system of the nonlinear equations, an in-house code based on finite difference method is developed and utilized. A parametric study is also carried out, and the results are discussed. The simulation results are in good agreement with published data. Results show a capacitive semicircle in the Nyquist plot, which is identical to the gas diffusion impedance as reported in literatures.

Keywords Solid oxide fuel cell · Electrochemical impedance spectroscopy · Impedance modeling · Gas diffusion impedance

R. Mohammadi (✉) · M. Ghassemi · M. H. Hamedi
Mechanical Engineering Department,
K.N. Toosi University of Technology,
Tehran, Iran
e-mail: rmohammadi@dena.kntu.ir

Y. Mollayi Barzi
Department of Mechanical Engineering, Kashan Branch,
Islamic Azad University,
Kashan, Iran

Nomenclature

C_g	Gas diffusion capacitance (F m^{-2})
$D_{i,j}$	Binary diffusivity between species i and j (m^2 s^{-1})
F	Faraday's constant (96,484.56 C mol^{-1})
f	Frequency (Hz)
f_g	Relaxation frequency (Hz)
g	Gibbs free energy (J mol^{-1})
H_{ch}	Channel height (m)
i	Current density (A m^{-2})
i_{total}	Total current density (A m^{-2})
$i°$	Exchange current density (A m^{-2})
$i_{excitation}$	Response amplitude (A m^{-2})
L	Cell length (m)
M_i	Species molecular mass (kg $kmol^{-1}$)
P	Total pressure (pa)
p_i^*	Partial pressure of reactants and products in the bulk flow (pa)
p_i	Partial pressure of reactants and products at the reaction sites (pa)
R	Universal gas constant (8.314 m^3kpa $kmol^{-1}$ K^{-1})
R_g	Gas diffusion resistance (Ω m^2)
R_{ct}	Electrode charge-transfer resistance (Ω m^2)
S_i	Volume-specific mass production rates of species i (kg m^{-3} s^{-1})
s_i	Area-specific mole production rates of species i (mol m^{-2} s^{-1})
T	Temperature (K)
V_{cell}	Actual cell voltage (V)
V_{nernst}	Nernst voltage (reversible open circuit voltage) (V)
$V_{nernst,t}$	True theoretical reversible voltage of the cell (V)
V_i	Special Fuller diffusion volume
W	Unit cell width (m)
W_{ch}	Channel width (m)
W_{rib}	Rib width (m)
y_i	Species mass fraction

y_i^*	Inlet species mass fraction
Y	Complex admittance (Ω^{-1})
Z	Complex impedance (Ω)

Greek symbols

ρ	Gas density (kg m^{-3})
η_{conc}	Concentration overvoltage (V)
η_{act}	Activation overvoltage (V)
η_{ohm}	Ohmic overvoltage (V)
η_{anode}	Anode overvoltage (V)
η_{steady}	Steady state overvoltage (V)
$\eta_{excitation}$	Excitation amplitude (V)
θ	Phase shift
τ	Time period (S)

Introduction

A fuel cell generates electrical power through an electrochemical reaction by converting chemical energy of a fuel into electrical energy. Fuel cells have higher efficiency compared to conventional combustion engines due to the fact that their efficiency avoids the limitations of Carnot cycle. In addition, the fuel cell itself has no moving part that makes it quiet and reliable. Furthermore, they have lower pollutant emissions, lower equipment maintenance, and higher power density [1]. Solid oxide fuel cells (SOFCs) are one of the fuel cell types that operate between 600 °C and 1,100 °C due to the low ionic conductivity of electrolytes such as yttria-stabilized zirconia (YSZ) at lower temperatures. In this type of fuel, cell oxidation of hydrogen and reduction of oxygen produce the electricity, water, and heat. SOFCs can be used in a wide range of applications. They appear suitable for stationary electricity generation, both for power plant scales and for small residential applications (combined heat and power generation) [2].

In order to improve the efficiency of the fuel cells, better understanding of the electrochemical reactions and mass transport in the fuel cell is essential. Therefore, it is useful to numerically analyze the experimental results of SOFCs. Various studies with different levels of sophistication on dynamic modeling of the SOFCs have been published [3–9]. Achenbach [3, 4] developed a mathematical model to simulate the dynamic operation of a planar SOFC. He investigated the transient cell performance due to a load change. Sedghisigarchi and Feliachi [5] combined heat transfer dynamics and species dynamics to form a new dynamic model. Xue et al. [6] considered a one-dimensional transient model for heat and mass transfer simulation assuming an electrical circuit includes the ohmic resistances and capacitors for the energy storage mode of operation. Chaisantikulwat et al. [7] obtained dynamic model of a planar SOFC and determined the voltage responses to step changes in the fuel concentration and load current. Mollayi Barzi et al. [8, 9] developed a two-dimensional transient model of a tubular SOFC using the control volume approach. This model predicted the cell output voltage as well as the state variables (pressure, temperature, and species concentration). The developed model determined the cell electrical and thermal responses to the variation of load current [8], and the cell heat-up rate for hot input gases as well as the start up time of the SOFC [9].

On the other hand, the electrochemical impedance spectroscopy (EIS) is a powerful non-destructive tool for materials characterization, transport properties investigation, and for obtaining the contribution of each loss in SOFCs [10]. Most of the published papers in the area of SOFCs impedance spectroscopy have reported the experimental results [11–14]. Initially, EIS measurements were mainly used to determine the conductivity of the SOFC components such as electrolyte and electrode materials [11]. Wagner et al. [12] presented the EIS measurements of polymer electrolyte fuel cells as well as SOFCs. The measured EIS was simulated with an equivalent circuit which enabled the calculation of the individual voltage losses in the fuel cell. The experiment not only determined the charge transfer arcs but also the diffusion arc of the low frequency region of the cells. A gas conversion impedance model for SOFC anodes was derived by Primdahl and Mogensen [13]. In this study, a simple continuously stirred tank reactor model was utilized. The model illustrated the anode EIS measurements with the reference electrode. The results were compared to the actual EIS measurements. In another study, Primdahl and Mogensen [14] measured the gas diffusion impedance in different setups to analyze and compare the correlation between the gas diffusion impedance and geometry parameters. Primdahl and Mogensen results showed an extra arc in impedance spectra which is called gas conversion or gas diffusion impedance. In order to analyze the experimental results of EIS, simulation of electrochemical impedance spectra is essential. Several researchers have developed SOFC impedance models. The experimental and numerical EIS study for anode reaction mechanisms was presented by Bieberle and Gauckler [15]. In this study, a series of steps for the overall electrochemical oxidation of hydrogen were proposed. Bessler [16] presented a new computational method for impedance simulations of SOFCs based on the Bieberle and Gauckler [15] proposed mechanisms. The suggested method was based on transient numerical simulations. In two other studies [17, 18], Bessler used the previous proposed model [16] for two different SOFC geometries. Kato et al. [19] also presented experimental results for SOFC impedance. In their study, the cell impedance was measured by varying the fuel utilization and gas flow rate. Takano et al. [20] presented a theoretical simulation based on an electrical circuit that modeled the electrochemical impedance of commercially available SOFCs under practical power generation conditions. Gazzarri and Kesler [21, 22] developed a finite element model to simulate the steady state and

impedance behavior of a SOFC in order to predict the impact of diverse degradation mechanisms on the impedance spectra. This model results suggested that electrode delamination can be detected minimally invasively by using EIS. Hofmann and Panopoulos [23] presented a detailed mathematical model based on physicochemical equations coupled with a multi-component gas diffusion mechanism for simulation of electrochemical impedance spectra. This model was built and implemented on the commercially available modeling and simulations platform gPROMS™. Based on mentioned researches, the experimental impedance spectra of the SOFC anode show two dominant features: a high-frequency process (1–10 kHz) associated with electrochemistry and a low-frequency process (~10 Hz) associated with gas diffusion in the anode channels [13, 14]. This feature results in a capacitive semicircle in Nyquist plot. The present study investigates the SOFC anode impedance by analyzing the latter feature.

All of the mentioned researches on dynamic modeling of SOFCs [3–9] mainly concern about SOFC transient response under step changes of voltage or current. Although in EIS experiments, impedance spectra were obtained by imposing a harmonic excitation to the cell. Therefore, in order to simulate the cell impedance in time domain, cell response to harmonic excitation is required. This is the first time to our knowledge that SOFC response under sinusoidal excitation is reported, which would be useful for electrochemical impedance spectra simulation. Moreover, in comparison with published papers in the field of EIS modeling [11–23], a detailed discussion on sinusoidal responses is performed in this paper, and the relation between the sinusoidal responses and the impedance spectra is investigated. The present model will take into account the transport phenomena in anode channel because mass transport of reactants and products has a strong effect on the performance of the SOFCs and influences the electrochemical impedance spectra in low-frequency region. The obtained impedance of SOFC anode is identical to gas diffusion impedance reported by literatures [13, 14]. The present model has the capability of predicting the response of linear small excitations as well as nonlinear large excitations. Because the model is based on physical laws and impedance, simulation is done in time domain. Therefore, all nonlinearities are maintained. In addition, the developed simulation code has the capability to be used in studying the effects of various parameters on the cell performance and the electrochemical impedance spectra of SOFC. Therefore, a parametric study is also carried out, and the results are discussed in detail.

Model description

The schematic diagram of the planar SOFC is depicted by Fig. 1. As shown, the hydrogen fuel passes through the anode channel. The numerical values used for simulation are given in Tables 1 and 2.

Electrochemical model

The overall SOFC reaction and the electrochemical oxidation reaction at the anode for hydrogen fuel are as follows, respectively:

$$H_2 + 1/2O_2 \rightarrow H_2O \tag{1}$$

$$H_2 + O^{2-} \rightarrow H_2O + 2e^- \tag{2}$$

The Nernst equation, which is used to determine the Nernst voltage (electromotive force (EMF)) of an electrochemical reaction, for SOFC is as follows [2]:

$$V_{\text{nernst}} = \frac{-\Delta g_f^\circ}{2F} + \frac{RT}{2F}\ln\left(\frac{p^*_{H_2} p^{*\,1/2}_{O_2}}{p^*_{H_2O}}\right) \tag{3}$$

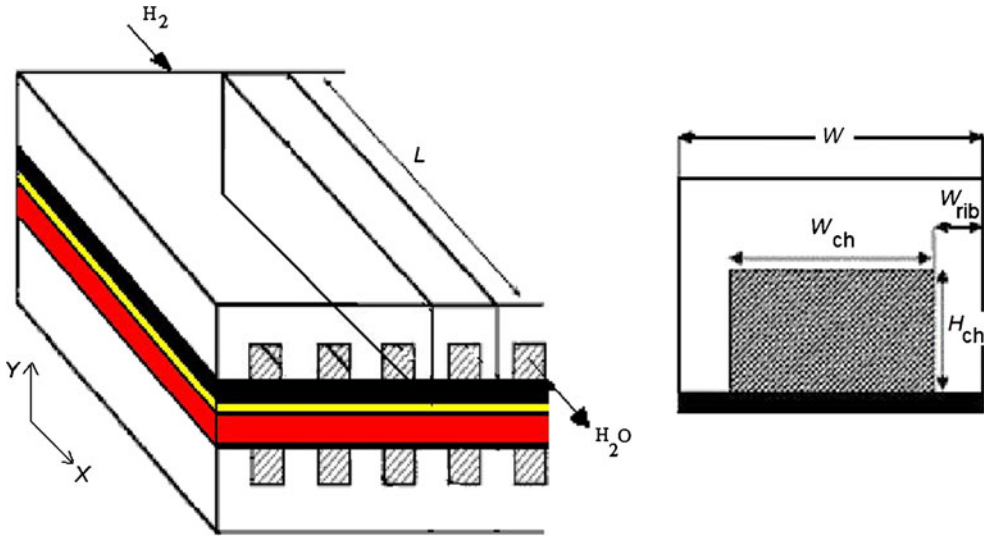

Fig. 1 Schematic diagram of a planar SOFC and computational domain

Table 1 Dimensions of the SOFC [7]

Element	Size (mm)
Cell length (L)	19
Unit cell width (W)	2
Channel width (W_{ch})	1
Channel height (H_{ch})	1
Rib width (W_{rib})	0.5

where p_i^* denotes the partial pressure of reactants and products in the bulk anodic and cathodic flows.

The actual SOFC voltage (V_{cell}) that is obtained by the cell is lower than its Nernst voltage. This is due to the overvoltages or polarizations (η). The overvoltages in SOFCs are caused by three main sources: (1) activation overvoltage (η_{act}), (2) ohmic overvoltage (η_{ohm}), and (3) concentration overvoltage (η_{conc}):

$$V_{cell} = V_{nernst} - \eta_{act} - \eta_{ohm} - \eta_{conc} \tag{4}$$

Concentration overvoltage is related to this fact that in proximity of the reacting sites in the electrodes, the concentration of reactants and products of the electrochemical reaction is different from the concentration in the bulk flow of the gases due to mass transport. Therefore, the true theoretical reversible voltage of the cell must be calculated by taking into account the reactant and product concentrations occurring in proximity of the reaction sites:

$$V_{nernst,t} = \frac{-\Delta g_f^\circ}{2F} + \frac{RT}{2F}\ln\left(\frac{p_{H_2} p_{O_2}^{1/2}}{p_{H_2O}}\right) \tag{5}$$

where p_i denotes the reactant and product partial pressure at the reaction sites. The difference between Eqs. 3 and 5 gives the concentration overvoltage:

$$\eta_{conc} = \frac{RT}{2F}\ln\left(\frac{p_{H_2}^* p_{H_2O}}{p_{H_2} p_{H_2O}^*}\right) + \frac{RT}{2F}\ln\left(\frac{p_{O_2}^*}{p_{O_2}}\right)^{1/2} \tag{6}$$

It is noted that the first term of Eq. 6 represents the anodic concentration overvoltage and the second term is the cathodic one. The activation overvoltage is determined from the Butler–Volmer equation for a symmetric two-electron transfer as follows [2]:

$$i = i^\circ\left\{\exp\left(\frac{F}{RT}\eta_{act}\right) - \exp\left(-\frac{F}{RT}\eta_{act}\right)\right\} \tag{7}$$

In the present study, the anode overvoltage (η_{anode}) of a SOFC is analyzed while the electrolyte and cathode overvoltage is ignored. Moreover, anode ohmic overvoltage is neglected due to the high anode electronic conductivity. Furthermore, concentration overvoltage within the porous anode is ignored. Therefore, the obtained results present anodic losses including both concentration overvoltage in anode channel and activation overvoltage. The anode overall loss is given by:

$$\eta_{anode} = \eta_{act} + \eta_{conc} \tag{8}$$

where the anodic concentration overvoltage in terms of the mass fraction of the gases becomes as follows:

$$\eta_{conc} = \frac{RT}{2F}\ln\left(\frac{y_{H_2}^* y_{H_2O}}{y_{H_2} y_{H_2O}^*}\right) \tag{9}$$

Combining Eqs. 7–9 yields:

$$i = i^\circ\left\{\left(\left(\frac{y_{H_2O} y_{H_2}^*}{y_{H_2} y_{H_2O}^*}\right)^{-1/2}\exp\left(\frac{F}{RT}\eta_{anode}\right)\right) - \left(\left(\frac{y_{H_2O} y_{H_2}^*}{y_{H_2} y_{H_2O}^*}\right)^{1/2}\exp\left(-\frac{F}{RT}\eta_{anode}\right)\right)\right\} \tag{10}$$

Table 2 The characteristics of the SOFC

Description	Value
Anode inlet pressure (atm) [7]	1
Cell temperature [7]	750 °C
Hydrogen inflow mass fraction	97 %
Water inflow mass fraction	3 %
Hydrogen diffusivity ($m^2\ s^{-1}$)	7.9×10^{-4}
Anode exchange current density ($A\ m^{-2}$)	4.408×10^{3}

Mass transfer model

The mass transfer along the anode channel is simulated using species conservation equation. In EIS experiments, the impedance of SOFCs is often obtained by single chamber setups and symmetrical cells. So, there is only diffusion transport in anode channel. In the present model, it is assumed that gases behave as ideal gases, and the total pressure and temperature are assumed to be constant through the entire electrode. There is no net change in the number of moles in gas phase in anode due to the electrochemical reaction (Eq. 2). Accordingly, constant total pressure assumption is quite reasonable. The one-

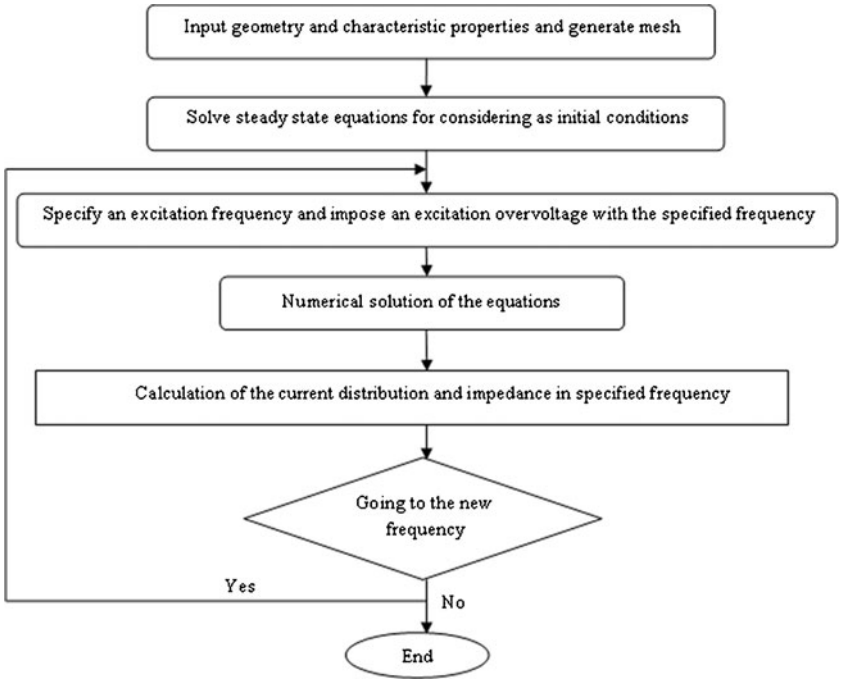

Fig. 2 Flowchart of the electrochemical impedance simulation process

dimensional species conservation equation when the diffusive mass flux is modeled by Fick's law is given by:

$$\frac{\partial(\rho y_{\mathrm{i}})}{\partial t} = \frac{\partial}{\partial x}\left(\rho D_{\mathrm{i,j}} \frac{\partial y_{\mathrm{i}}}{\partial x}\right) + S_{\mathrm{i}} \tag{11}$$

where S_{i} is the volume-specific mass production rates of species i. The area-specific mole production rates of species (s_{i}) are given by the faradaic current due to the electrochemical reaction of hydrogen fuel as follows:

$$s_{\mathrm{H_2}} = -\frac{i}{2F} \tag{12}$$

$$s_{\mathrm{H_2O}} = \frac{i}{2F} \tag{13}$$

The relation between volume-specific mass production rates of species i and area-specific mole production rates of species i according to cell geometry (Fig. 1) is given by:

$$S_{\mathrm{i}} = s_{\mathrm{i}} M_{\mathrm{i}} \left(\frac{W}{W_{\mathrm{ch}} H_{\mathrm{ch}}}\right) \tag{14}$$

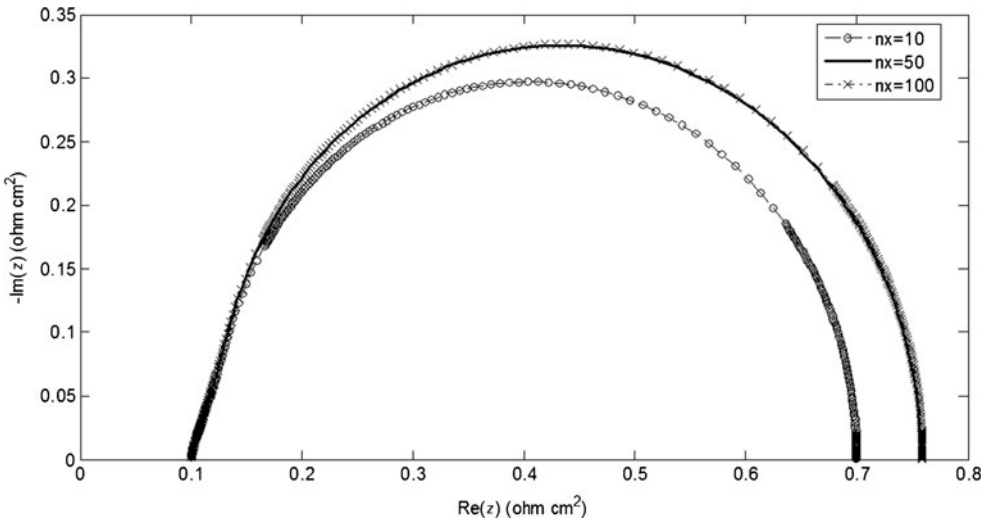

Fig. 3 Electrochemical impedance spectra for different grid numbers

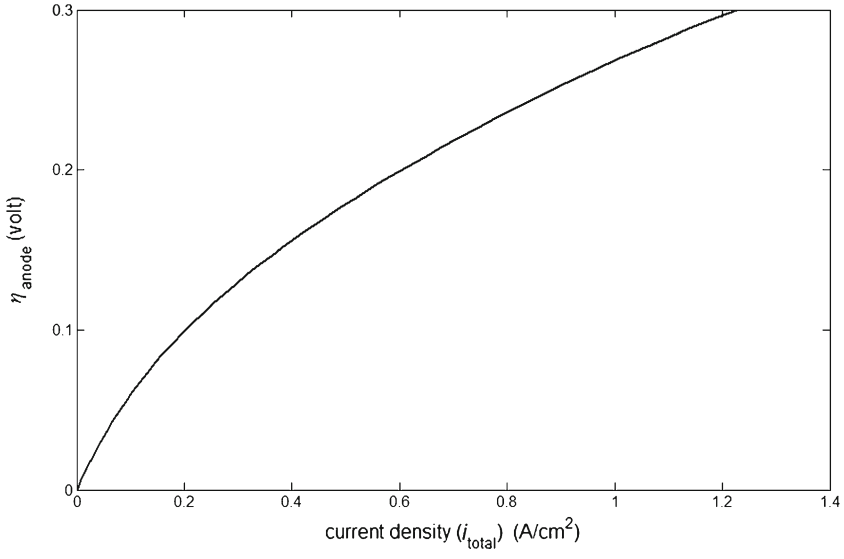

Fig. 4 Steady state current overvoltage graph

Combining Eqs. 10–12 and 14 yields hydrogen species equation as follows:

$$\frac{\partial(\rho y_{H_2})}{\partial t} = \frac{\partial}{\partial x}\left(\rho D_{H_2-H_2O}\frac{\partial y_{H_2}}{\partial x}\right) + \left(-\frac{i^{\circ} M_{H_2} W}{2FW_{ch}H_{ch}}\right)\left\{\left(\left(\frac{y_{H_2O}y^*_{H_2}}{y_{H_2}y^*_{H_2O}}\right)^{-1/2}\exp\left(\frac{F}{RT}\eta_{anode}\right)\right) - \left(\left(\frac{y_{H_2O}y^*_{H_2}}{y_{H_2}y^*_{H_2O}}\right)^{1/2}\exp\left(-\frac{F}{RT}\eta_{anode}\right)\right)\right\} \quad (15)$$

At the channel inlet, the species concentrations are set as boundary conditions. Furthermore, the fully developed assumption is considered at the outlet of the channel.

At high temperature, all the gaseous components are assumed to behave as ideal gases:

$$p = \rho RT\sum y_i/M_i \quad (16)$$

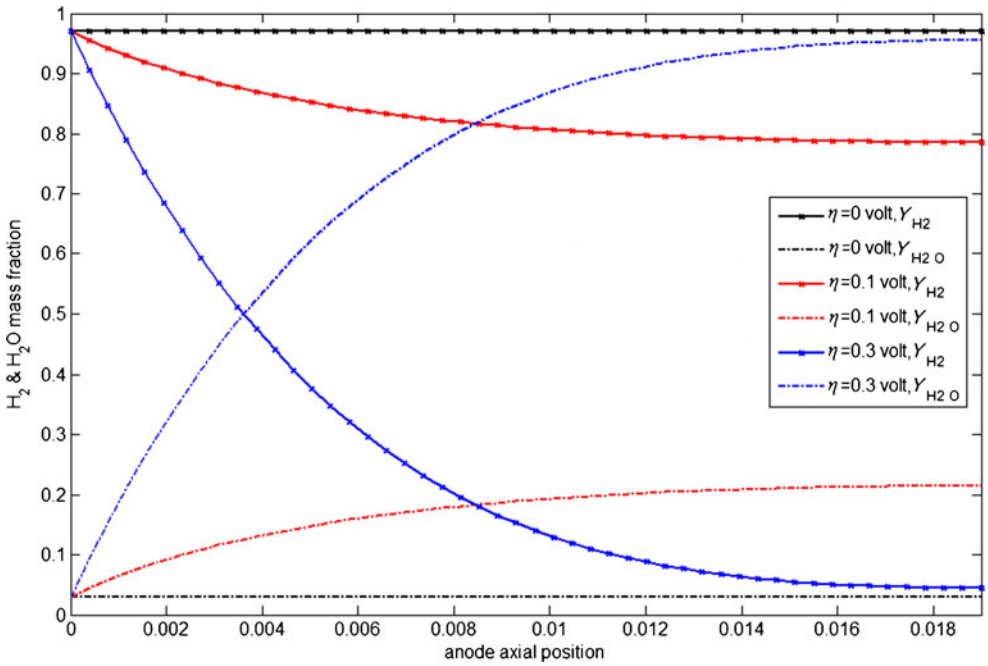

Fig. 5 Axial distribution of hydrogen and water mass fraction in anode channel for different cell values of overvoltages

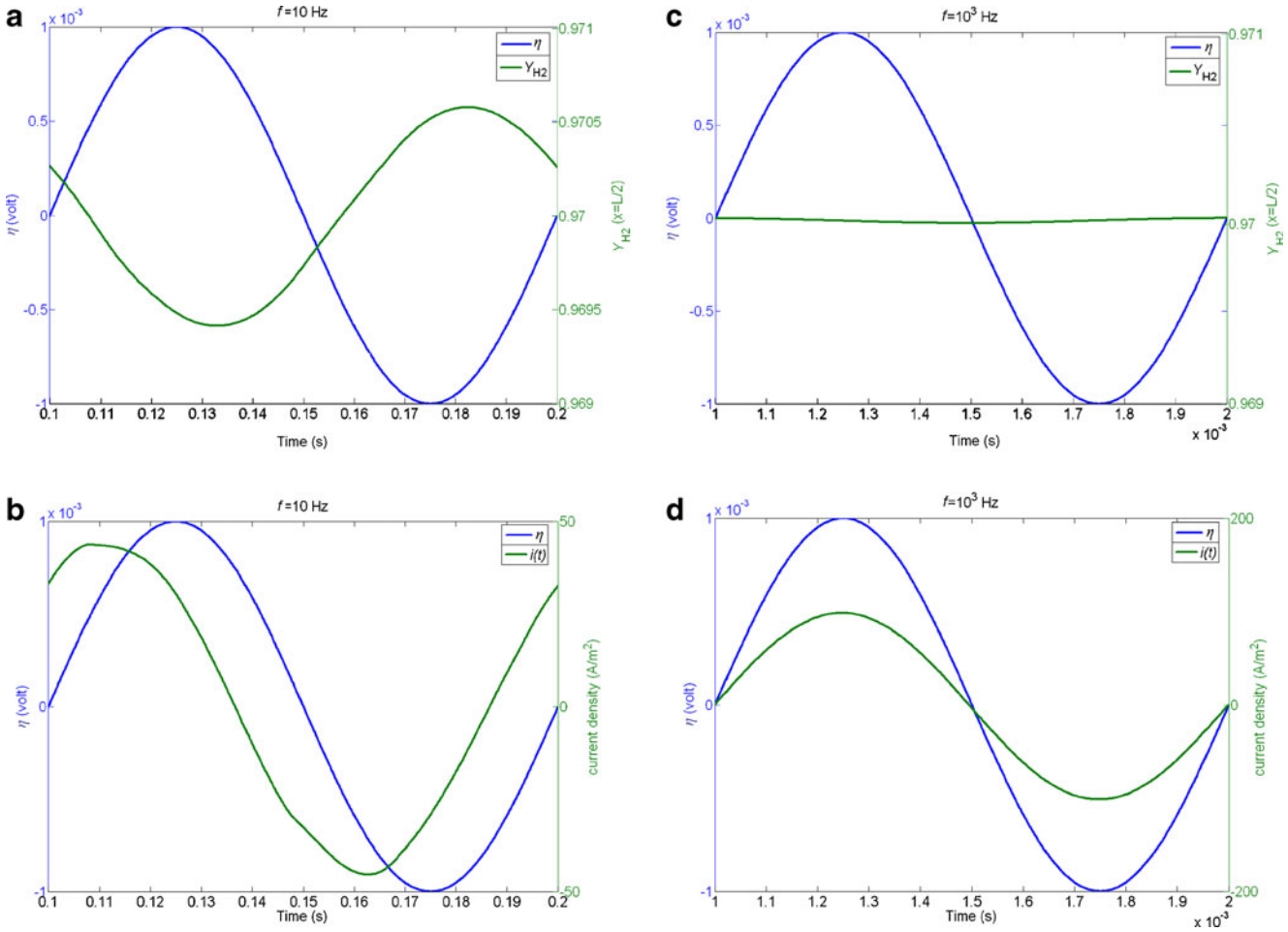

Fig. 6 SOFC anode response to sinusoidal excitation at the middle of channel length for η_{steady}=0 V, $\eta_{excitation}$=0.001 V, and different frequencies

The binary diffusivity between species i and j is determined by [24]:

$$D_{i,j} = \frac{0.00143\ T^{1.75}}{p\ M_{i,j}^{0.5}\left[V_i^{1/3} + V_j^{1/3}\right]^2} \tag{17}$$

where V_i, V_j are special Fuller diffusion volume [24], and $M_{i,j}$ is given by:

$$M_{i,j} = 2\left[\left(\frac{1}{M_i}\right) + \left(\frac{1}{M_j}\right)\right]^{-1} \tag{18}$$

The total current density (i_{total}) is determined by:

$$i_{total} = \frac{1}{L}\int_0^L i(x,t)\mathrm{d}x \tag{19}$$

Electrochemical impedance model

The complex impedance (Z) and complex admittance (Y) are determined by Eqs. 20 and 21, respectively [10]:

$$Z = \frac{1}{Y} \tag{20}$$

$$Y = \frac{i_{excitation}}{\eta_{excitation}}(\cos\theta + j\sin\theta) \tag{21}$$

In Eq. 21, $\eta_{excitation}$ is excitation amplitude of imposed overvoltage. For the impedance simulation, a harmonically varying overvoltage is imposed to the anode overvoltage in Eq. 15 as follows [16]:

$$\eta_{anode} = \eta_{steady} + \eta_{excitation}\sin(2\pi ft) \tag{22}$$

where η_{steady} is the time-invariant contribution and represents the steady state overvoltage, and f is the excitation frequency.

Furthermore, in Eq. 21, θ is the phase angle by which the observed cell current is shifted from the imposed overvoltage, and $i_{excitation}$ is the amplitude of harmonic response and is given by:

$$i(t) = i_{steady} + i_{excitation}\sin(2\pi ft + \theta) \tag{23}$$

where $i(t)$ is the observed cell transient current density for when the steady oscillating response is established (usually

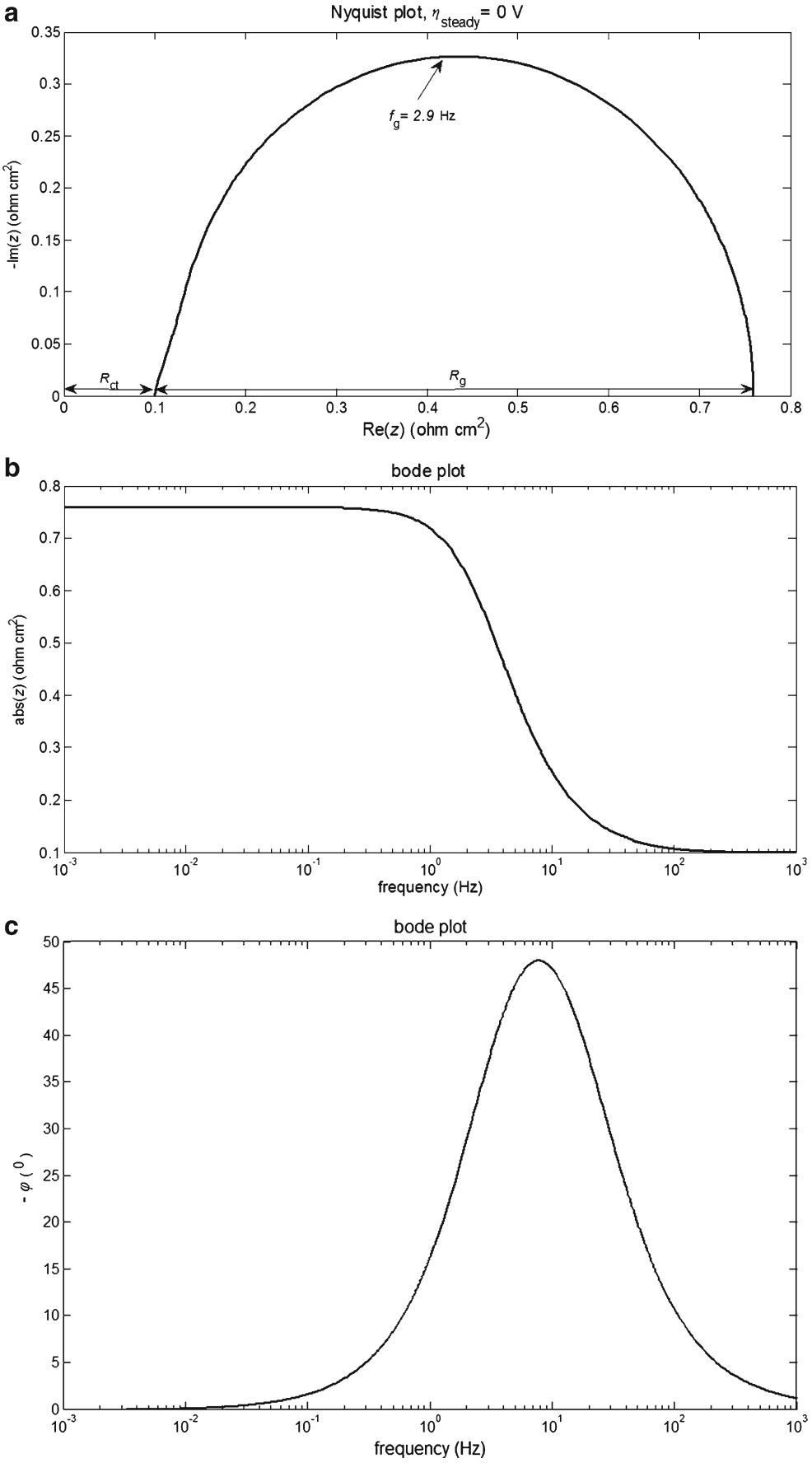

Fig. 7 Electrochemical impedance spectra: (**a**) Nyquist plot (**b**, **c**), Bode plots

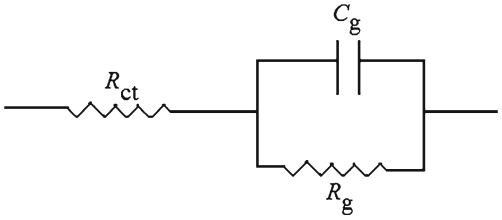

Fig. 8 Equivalent circuit for anode

after a few periods). The harmonic response takes places when the excitation amplitude is sufficiently small. Equation 23 can be rewritten alternatively as:

$$i(t) = i_{\text{steady}} + i_{\text{excitation}}\{\sin(2\pi ft)\cos\theta + \cos(2\pi ft)\sin\theta\} \quad (24)$$

Multiplying Eq. 24 by $\sin(2\pi\ ft)$ and $\cos(2\pi\ ft)$ and integrating over a period ($\tau = 1/f$) yields the following relationships:

$$i_{\text{excitation}}\cos\theta = \frac{2}{\tau}\int_{t=0}^{\tau} i(t)\sin(2\pi ft)\mathrm{d}t \quad (25)$$

$$i_{\text{excitation}}\sin\theta = \frac{2}{\tau}\int_{t=0}^{\tau} i(t)\cos(2\pi ft)\mathrm{d}t \quad (26)$$

Therefore, based on Eqs. 21, 25, and 26, the real part (Y') and the imaginary part (Y'') of admittance are given by:

$$Y' = \frac{2}{\tau.\eta_{\text{excitation}}}\int_{t=0}^{\tau} i(t)\sin(2\pi ft)\mathrm{d}t \quad (27)$$

$$Y'' = \frac{2}{\tau.\eta_{\text{excitation}}}\int_{t=0}^{\tau} i(t)\cos(2\pi ft)\mathrm{d}t \quad (28)$$

Simulation procedure

The flowchart for the overall simulation process of the anode impedance spectra is shown in Fig. 2. In order to solve the system of the nonlinear equations, an in-house code based on finite difference method is developed by MATLAB software. The developed simulation code has the capability to be used in studying the steady state and sinusoidal behavior of SOFCs, simulating the electrochemical impedance spectra, as well as investigating the effects of various parameters on the electrochemical impedance spectra of SOFCs. The simulation is based on finite difference method. The discretized equations form a differential algebraic system, which is solved by the method of lines algorithm [25]. The initial steady state is achieved by setting the $\eta_{\text{excitation}}$ equal to zero, and the steady state operation results are set as initial values. Then at a specified frequency, the governing equations are time integrated to determine the transient current ($i(t)$) of the system. Finally, the electrochemical impedance of assumed frequency is obtained. The process for a range of frequencies (10^{-3} to 10^{3} Hz with 10 impedance points per frequency decades) is repeated until an impedance spectrum is obtained. It is noted that the relaxation frequencies are determined with 100 points/decade resolution. The computational domain is discretized by a 50-uniform grid in longitudinal direction, while 400 values of time are calculated within one period. The grid independency of the results is examined and insured as shown in Fig. 3. As shown, results are identical for 50 and 100 grids. Therefore, a 50-grid domain is utilized.

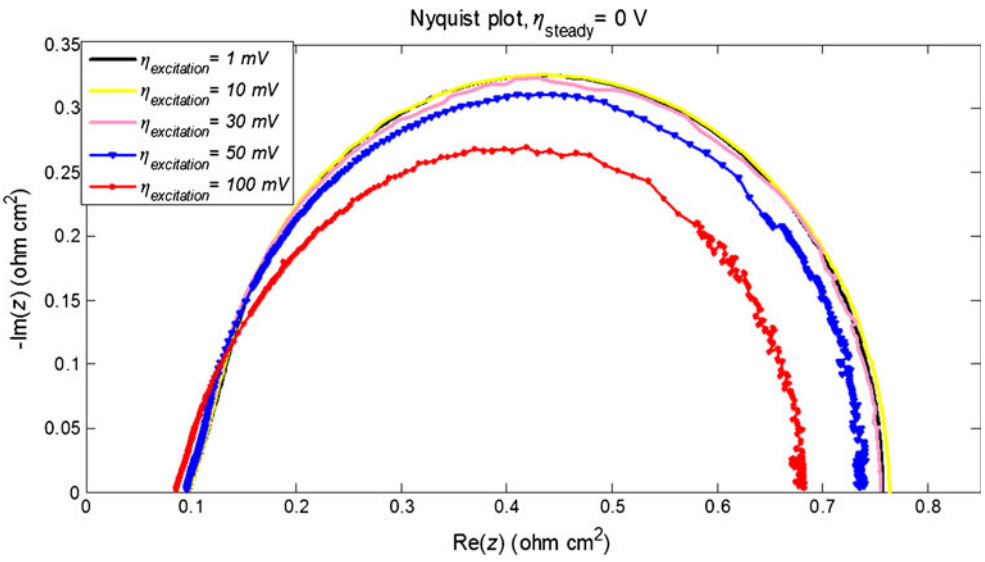

Fig. 9 Electrochemical impedance spectra for different excitation amplitude

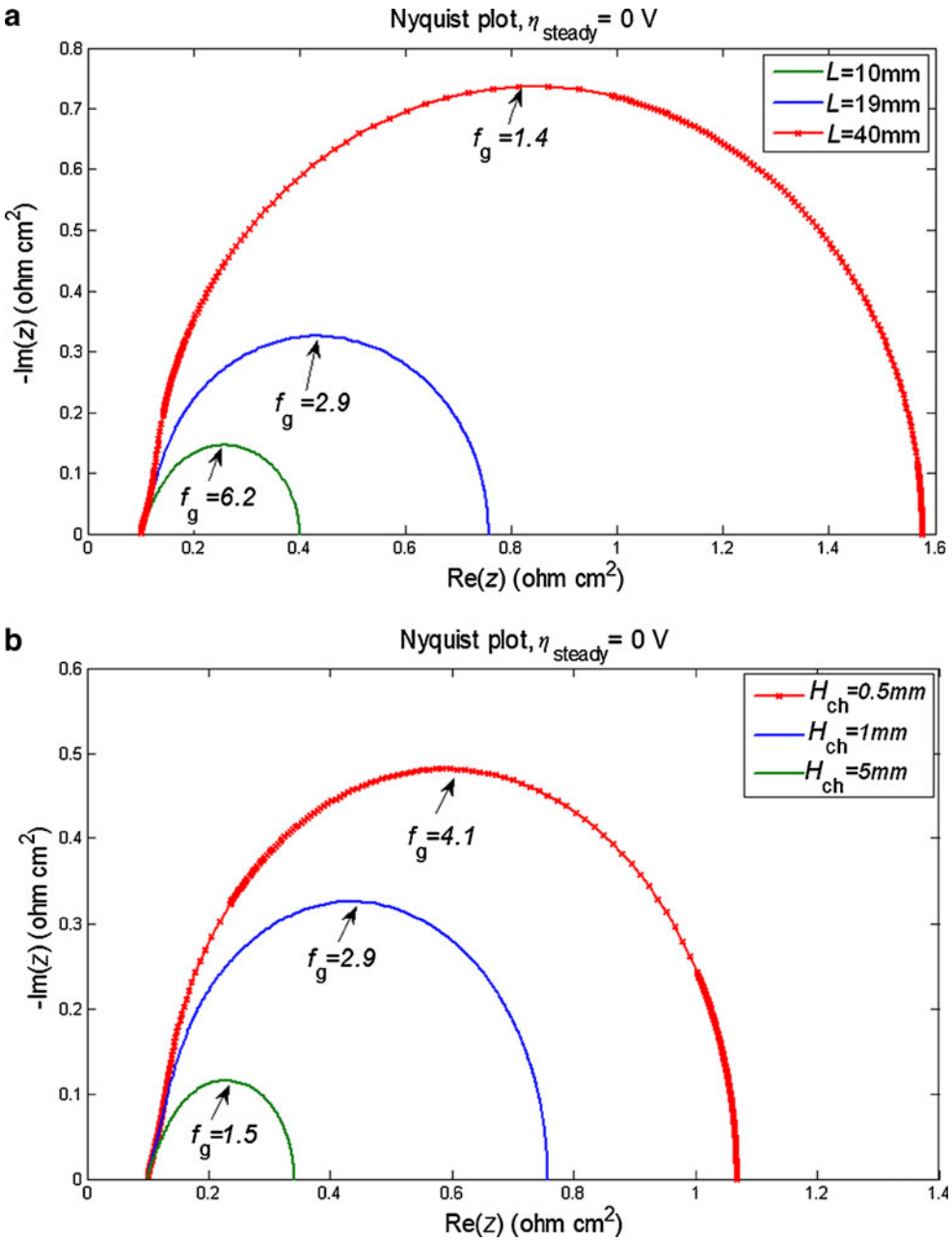

Fig. 10 Electrochemical impedance spectra for different cell dimensions

Results and discussion

Steady state results

Figure 4 depicts the steady state current–overvoltage graph. Here, the anode overvoltage is plotted versus the total current density. This figure could be considered as polarization curve ($V_{cell} = V_{nernst} - \eta_{anode}$). The figure shows the typical polarization curves shape, since it has a parabolic behavior close to open circuit (η_{anode}=0) and then the curve is quite linear.

Figure 5 illustrates the hydrogen and vapor mass fraction distribution along the length of the fuel channel for various values of overvoltages. The inlet mass fraction of hydrogen is assumed 97 %. As shown, the mass fraction of hydrogen decreases while the mass fraction of vapor increases along the fuel channel. This is due to consumption of hydrogen and production of vapor from the anode wall. At open circuit voltage, there is no consumption of hydrogen, and the mass fractions remain constant. While for higher overvoltages (η_{anode}=0.1, 0.3 V), the consumption of hydrogen increases and

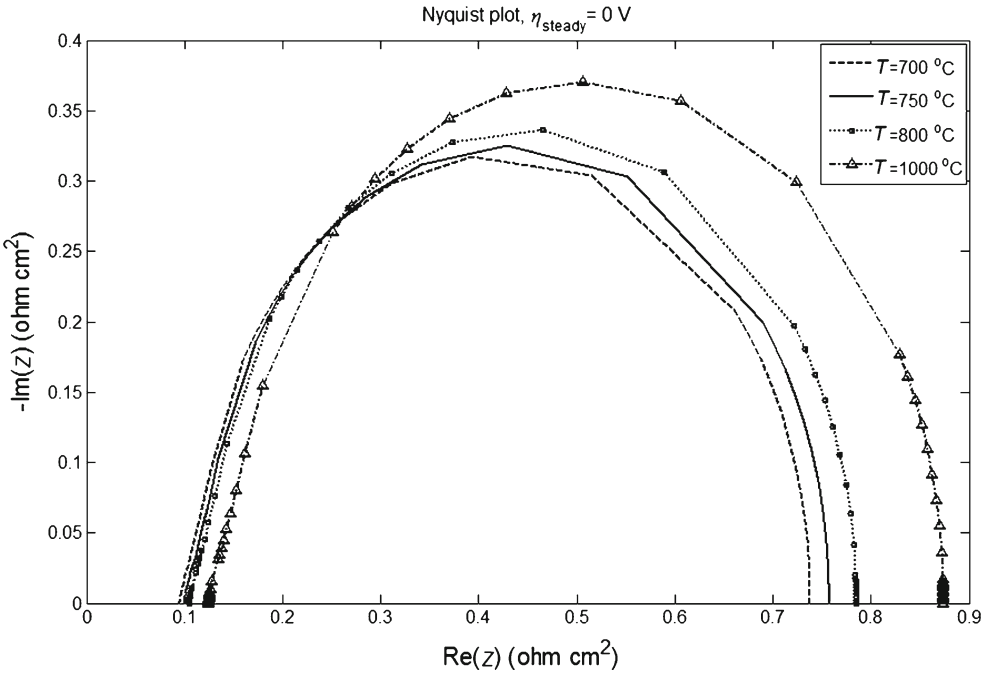

Fig. 11 Electrochemical impedance spectra for different temperatures

causes the hydrogen mass fraction to decrease. Therefore, the vapor mass fractions increase.

Cell response to sinusoidal excitation

Dynamic periodic variation of applied overvoltage, hydrogen mass fraction, and current density of two different frequencies are shown in Fig. 6a–d. These parameters are plotted for one period during simulation. As shown by Fig. 6a, c, sinusoidal excitation causes harmonic concentration changes of the chemical species. In addition, by increasing the frequency, the range of hydrogen mass fraction changes decreases. When the frequency of applied excitation overvoltage is higher than the frequency that is associated to response time of the gas through the channel, the concentration changes of the chemical species by the applied excitation overvoltage become

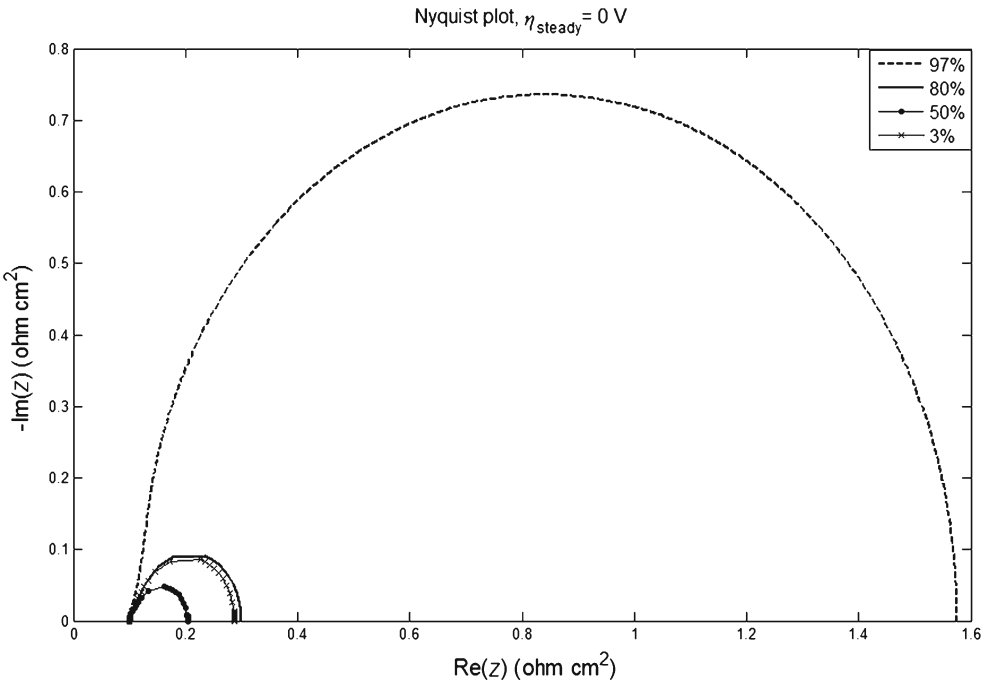

Fig. 12 Electrochemical impedance spectra for different inlet fuel concentrations

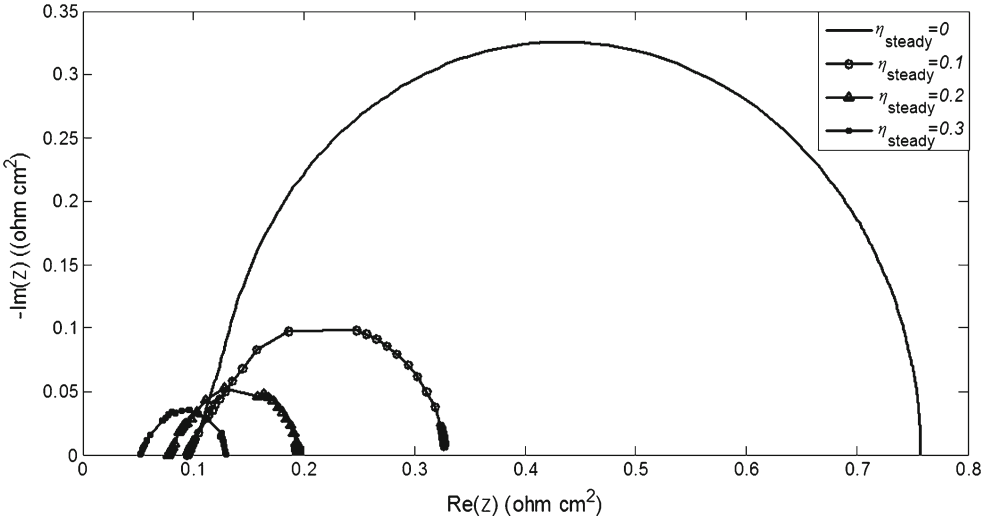

Fig. 13 Electrochemical impedance spectra for different steady state overvoltages

nearly zero. Indeed, at high frequencies, variables are almost constant because they are not sensitive to the high frequency.

In addition, phase shift and amplitude difference between overvoltage and current are depicted in Fig. 6b, d. As shown, a phase shift between overvoltage and current is appeared which is due to capacitive behavior described by the mass transfer equations. Because of this behavior, imaginary impedance is generated. By increasing the frequency, the phase shift between overvoltage and current decreases.

Impedance spectra

Obtained responses to the harmonically varying overvoltages could be used for the electrochemical impedance simulation. All presented results in the following sections are obtained using the parameters given in Tables 1 and 2. In addition, the excitation amplitude is considered to be 1 mV. Moreover, the electrode charge-transfer resistance (R_{ct}) at open-circuit conditions and 97 % inlet H_2 is equal to 0.1 Ω cm^2 as observed in experiments [13]. R_{ct} at open-circuit condition is given by [10]:

$$R_{ct} = \frac{RT}{2Fi^{\circ}} \tag{29}$$

Therefore, to achieve 0.1 Ω cm^2 for R_{ct}, the exchange current density is set equal to 0.4408 A/cm^2. Figure 7 depicts the impedance spectra for η_{steady}=0 V. The Nyquist plot consists of a semicircle with a relaxation frequency of 2.9 Hz (for which the imaginary part of impedance has a maximum value, f_g), gas diffusion resistance of about 0.66 Ω cm^2 (the difference between the low-frequency and the high-frequency real part, R_g), and gas diffusion capacitance of 0.08 F/cm^2 $\left(C_g = 1/\left(2\pi R_g f_g\right)\right)$. In other words, R_g is calculated from the intersections of the arc with the real axis. Also, the high-frequency intercept with the real axis corresponds to the charge-transfer resistance. The equivalent circuit of the spectrum is shown in Fig. 8.

The observed impedance feature is for anodic gas-phase concentration variations. Indeed, phase shift between input and output signals, which is observed in Fig. 6, is the origin of the impedance arc. Primdahl and Mogensen called this feature gas conversion or gas diffusion impedance [13, 14], and Bessler used the term gas concentration impedance for this feature [17]. This impedance feature is related to concentration polarization.

There is not much data published so far about experimental impedance spectroscopy of planar SOFCs. Thus, for verification purposes, the electrochemical impedance spectrum is compared to Primdahl and Mogensen results [13]. Primdahl and Mogensen reported experimental impedance spectra of single-chamber symmetrical electrodes in 97 % H_2 and 3 % H_2O at 1,000 °C and 1 atm pressure. In this experiment, electrode samples were broken down into ~5×5-mm squares and mounted between grids of Pt current collecting wires, where the wires were 0.3 mm in diameter with a grid distance of ~1.5 mm. According to channel geometry (Fig. 1), these values correspond to channel length of 5 mm, cell width of 1.5 mm, and channel height of 0.3 mm. Using these parameters, the relaxation frequency of the gas diffusion process is 60 Hz, and the gas diffusion resistance is 0.05 Ω cm^2. These values are almost equal to Primdahl and Mogensen observation of R_g~0.05 Ω cm^2 and f_g~70 Hz.

SOFC physics and chemistry are nonlinear, but impedance spectra are determined by imposing sufficiently small harmonic excitation in order to cause a harmonic response. The impedance simulation based on modeling in time domain retains the full nonlinear behavior of the SOFC. As shown in Fig. 9, simulation results show that when excitation amplitude changes from 1 to 30 mV, the impedance spectra do not change. For 50 and 100 mV excitation amplitude, changes in gas diffusion impedance and electrode charge-transfer

resistance are observed, which are due to the nonlinear behavior of the system. Consequently, the coupled electrochemistry and gas diffusion phenomena simulated in this work behave linearly for excitation amplitudes up to 30 mV. Furthermore, with increasing excitation amplitude, the numerical simulation code becomes unstable, especially in low frequencies, and the shape of the impedance arc changes.

Parametric study

The developed simulation code has the capability to be used in studying the effects of various parameters on the electrochemical impedance spectra of SOFC.

Effect of cell dimensions

Figure 10 depicts the variations of the calculated impedance versus different cell length (19 mm (base dimension), 10 mm, and 40 mm) and different channel height (1 mm (base dimension), 0.5 mm, and 5 mm). As shown, variation of fuel cell dimensions has a significant influence on the gas diffusion impedance. The diameter of the arcs changes with variation of the cell dimensions. This is due to mass transport inside the channel. As cell length increases and its height decreases, the gas diffusion resistance increases. In addition, reduction of the cell length and cell height will increase the relaxation frequency and shift the arc of gas diffusion impedance toward a higher frequency. This behavior is similar to Primdahl and Mogensen results [13]. However, the high frequency edge of the arcs is not affected by changing the cell dimensions. This is due to the behavior of the anode in high frequencies as shown in Fig. 6, where the variables are almost constant in the high frequencies.

Effect of temperature

Figure 11 illustrates the simulated impedance spectra for the different anode operating temperatures. R_{ct} is proportional to temperature (Eq. 29) and as shown decreases as temperature decreases. In addition, the gas diffusion resistance decreases as temperature decreases. This behavior was predicted in Primdahl and Mogensen model as well [13]. They showed that the gas diffusion resistance is proportional to the operating temperature of the anode in a SOFC. In fact, the temperature dependence of concentration overvoltage is complicated [2]. On one hand, it is expected that mass transport inside the channel decreases by temperature reduction (i.e., R_g increases) since diffusion coefficients decrease with temperature reduction (Eq. 17). On the other hand, as seen from Eq. 9, concentration overvoltage is proportional to temperature, which would mean R_g decreases with temperature reduction. In general, the concentration overvoltage is not a very strong function of temperature [2].

Effect of inlet fuel concentration

The impedance spectra at different inlet hydrogen concentrations are depicted in Fig. 12. As shown, the high frequency edge of the arcs is not affected by changing the inlet hydrogen concentration. This is due to the behavior of anode in high frequencies as shown in Fig. 6. However, the diameter of the arcs changes with variation of the inlet hydrogen concentration. The diameter becomes bigger as the inlet hydrogen concentration approaches either zero or 100 %. The minimum value of arc diameters takes place at 50 % inlet hydrogen concentration. This is due to the fact that based on Eq. 9, the gas diffusion overvoltage is minimum at 50 % inlet hydrogen concentration.

Effect of steady state overvoltage

Figure 13 shows the simulated impedance spectra at steady state overvoltages of η_{steady}=0, 0.1, 0.2, and 0.3 V. As shown, at each steady state overvoltage, one semicircle appears in the Nyquist plot. At high overvoltages, the gas diffusion impedance in cell reaches a minimum value. This is due to water vapor content of the gas in SOFC anode channel, which has a strong effect on the electrochemical characteristics of the cell. As overvoltage (current density) increases, the water production rate at the anode interface increases and R_g decreases. This behavior has been observed in experiments as well [12].

Conclusions

In this paper, simulation and analysis of the behavior of a SOFC anode under sinusoidal excitation is considered, and the steady state behavior and the frequency response are obtained. The obtained sinusoidal response is used as a base for the electrochemical impedance spectra simulation. To do this, a periodic voltage is imposed, and the response is utilized for impedance modeling. The strong emphasis of this study is on the mass transport phenomena in the anode channel, and its effect on electrochemical impedance spectra is investigated. Moreover, a detailed discussion on harmonic responses is performed in this paper, and the relations between sinusoidal responses and impedance spectra are investigated. In addition, the developed simulation code has the capability to be used in studying the effects of various parameters on the cell performance and the electrochemical impedance spectra of SOFC. Therefore, a parametric study is also carried out, and the results are discussed. The following results have been found:

- A phase shift between imposed overvoltage and obtained current is observed, which is the origin of the impedance arc.

- The channel diffusion causes a capacitive behavior in the form of a RC-type semicircle with low relaxation frequency and high capacitance in the Nyquist diagram, which is identical to the gas diffusion impedance as reported in literatures.
- The model has the capability of predicting the response of linear small excitation as well as nonlinear large excitation because the model is based on physical laws and simulation is based on modeling in time domain. Therefore, all nonlinearities are maintained.
- Variation of fuel cell dimensions has a significant influence on the gas diffusion impedance. As cell length increases or its height decreases, gas diffusion resistance increases. When the cell length is changed from 19 to 40 mm, the gas diffusion resistance changes from 0.66 to 1.57 Ω cm^2.
- Variations of inlet hydrogen concentrations are studied, and it is observed that the high frequency edge of the arcs is not affected by changing the inlet hydrogen concentration. However, the diameter of the arcs changes with the inlet hydrogen concentration. The minimum value of arc diameters takes place at 50 % inlet hydrogen concentration.
- The simulation results are in full qualitative and reasonable quantitative agreement with published data.

From the simulation results, it is found that the EIS simulation produces a tool for both analyzing experimental results of EIS and performance optimization of fuel cells. Therefore, EIS simulation will decrease the amount of costly experiments.

References

1. Larminie J, Dicks A (2003) Fuel cell systems explained, 2nd edn. Wiley, West Sussex
2. Singhal SC, Kendall K (2003) High temperature solid oxide fuel cells: fundamentals, design and applications. Elsevier Science, Oxford
3. Achenbach E (1994) Three-dimensional and time-dependent simulation of a planar solid oxide fuel cell stack. J Power Sources 49:333–348
4. Achenbach E (1995) Response of a solid oxide fuel cell to load change. J Power Sources 57:105–109
5. Sedghisigarchi K, Feliachi A (2004) Dynamic and transient analysis of power distribution systems with fuel cells part I. IEEE Energy Conver 19(2):423–428
6. Xue X, Tang J, Sammes N, Du Y (2005) Dynamic modeling of single tubular SOFC combining heat/mass transfer and electrochemical reaction effects. J Power Sources 142:211–222
7. Chaisantikulwat A, Goano CD, Meadows ES (2008) Dynamic modelling and control of planar anode-supported solid oxide fuel cell. J Comput Chem Eng 32:2365–2381
8. Mollayi Barzi Y, Ghassemi M, Hamedi MH (2009) A 2D transient numerical model combining heat/mass transport effects in a tubular solid oxide fuel cell. J Power Sources 192:200–207
9. Mollayi Barzi Y, Ghassemi M, Hamedi MH (2009) Numerical analysis of start-up operation of a tubular solid oxide fuel cell. J Hydrogen Energy 34:2015–2025
10. Macdonald JR (2005) Impedance spectroscopy—theory experiment and application, 2nd edn. Wiley, New York
11. Verkerk MJ, Burggraaf AJ (1983) Oxygen transfer on substituted ZrO2, Bi2O3, and CeO2 electrolytes with platinum electrodes. J Electrochem Soc 130:78–84
12. Wagner N, Schnurnberger W, Muller B, Lang M (1998) Electrochemical impedance spectra of solid-oxide fuel cells and polymer membrane fuel cells. Electrochim Acta 43(24):3785–3793
13. Primdahl S, Mogensen M (1998) Gas conversion impedance: a test geometry effect in characterization of solid oxide fuel cell anodes. J Electrochem Soc 145(7):2431–2438
14. Primdahl S, Mogensen M (1999) Gas diffusion impedance in characterization of solid oxide fuel cell anodes. J Electrochem Soc 146(8):2827–2833
15. Bieberle A, Gauckler L (2002) State-space modeling of the anodic SOFC system Ni, H2–H2O-YSZ. Solid State Ionics 146:23–41
16. Bessler W (2005) A new computational approach for SOFC impedance based on detailed electrochemical reaction–diffusion models. Solid State Ionics 176:997–1011
17. Bessler W (2006) Gas concentration impedance of solid oxide fuel cell anodes I. Stagnation point flow geometry. J Electrochem Soc 153(8):A1492–A1504
18. Bessler W, Gewies S (2007) Gas concentration impedance of solid oxide fuel cell anodes II. Channel geometry. J Electrochem Soc 154:B548–B559
19. Kato T, Nozaki K et al (2004) Impedance analysis of a disk-type SOFC using doped lanthanum gallate under power generation. J Power Sources 133:169–174
20. Takano K, Nagata S et al (2004) Numerical simulation of a disk-type SOFC for impedance analysis under power generation. J Power Sources 132:42–51
21. Gazzarri JI, Kesler O (2007) Non-destructive delamination detection in solid oxide fuel cells. J power sources 167:430–441
22. Gazzarri JI, Kesler O (2007) Electrochemical AC impedance model of a solid oxide fuel cell and its application to diagnosis of multiple degradation modes. J Power Sources 167:100–110
23. Hofmann Ph, Panopoulos KD (2010) Detailed dynamic solid oxide fuel cell modeling for electrochemical impedance spectra simulation. J Power Sources 195:5320–5339
24. Todd B, Young JB (2002) Thermodynamic and transport properties of gases for use in solid oxide fuel cell modeling. J Power Sources 110:186–200
25. Schiesser WE, Griffiths GW (2009) A compendium of partial differential equation models: method of lines analysis with Matlab, 1st edn. Cambridge University Press, New York